Thesis for the Degree of Licentiate of Engineering

Energy Efficient Longitudinal Control

by

RICKARD ARVIDSSON

CHALMERS
UNIVERSITY OF TECHNOLOGY

Division of Combustion and Propulsion Systems
Department of Mechanics and Maritime Sciences
Chalmers University of Technology
Gothenburg, Sweden 2018

Energy Efficient Longitudinal Control

RICKARD ARVIDSSON

Supervisor: Tomas McKelvey, Electrical Engineering
Examiner: Ingemar Denbratt, Mechanics and Maritime Sciences

Licenciate Thesis 2018:03
Division of Combustion and Propulsion Systems
Department of Mechanics and Maritime Sciences
Chalmers University of Technology
SE-412 96 Gothenburg
Telephone +46 31 772 1000

Cover: A vehicle with look-ahead sensors

Printed by Chalmers Reproservice
Gothenburg, Sweden 2018

Energy Efficient Longitudinal Control
RICKARD ARVIDSSON
Department of Mechanics and Maritime Sciences
Chalmers University of Technology

Abstract

Vehicles are contributing to global and local environmental problems as a result of fossil fuels. A majority of the combustion engine population is driven by fossil fuels and electrified vehicles are also to a large extent dependent on electricity production from fossil fuels. Emission legislation and standardized test methods have lead the development of technology for the automotive industry. Increased efficiency, improved combustion control and aftertreatment systems have created cleaner and more fuel efficient drivetrains. Authorities and publications have highlighted an increased gap between in-use and certified vehicle consumption and emissions because of the test-cycles current design. In order to address these differences authorities have conducted changes within the test methods from 2017 and forward and a new test-cycle WLTP is introduced including real-driving-emission test procedures. Decreasing the gap of real driving emissions and consumption can also be improved outside the legislative test-cycles using forward looking sensors, map data and statistical models.

The work considers controlling the drivetrain actuators more efficiently in a vehicle with predictive information. For this, dynamic programming is used to optimize engine speed trajectories during depletion mode for a series hybrid drivetrain. The result shows that choice of state and control signals has a direct impact on the engine speed trajectory and thereby the fuel consumption. Up to 21 % lower fuel consumption could be achieved for a series hybrid drivetrain compared to a rule based engine speed demand controller (along the best efficiency line) for the drivecycle analyzed. For a parallel hybrid drivetrain a DP method was compared to a heuristic strategy in order to determine the optimal discharge rate of the battery. In the simulation study done the DP method provided the best fuel consumption results. During evaluation of the physical tests the pre-optimized DP parameter set performed worse than the heuristic strategy. In the rig tests a fuel consumption reduction of 8 % was measured with the heuristic method, compared to a non predictive controller strategy. The DP algorithm provided 4 % reduction of fuel compared to a non predictive controller.

The work has also considered different modeling methods of a high voltage battery from recorded fleet data. One individual vehicle recorded battery pack current and voltage for one year. The recorded data was used to identify battery parameters for electric equivalent circuits. The measured current was used to calculate a reference voltage from the circuit equivalent parameters that was compared to the measured voltage. The best result was obtained for a single RC circuit model which obtained the highest average goodness of fit in voltage for the entire training data set.

Keywords: Drivetrain Optimization, Fuel Consumption, Hybrid, Dynamic Programming, DP, MPC, ITS

Acknowledgements

The years which have passed during my time as a PhD. student have probably been the most outstanding years in terms of technology shifts and disruption for the automotive industry in history. After five months as a PhD. student in September 2015, the Volkswagen diesel scandal was announced worldwide. The Environmental Protection Agency released test protocols from real driving which proved widespread illegal control and cheating outside the certification cycle performed by Volkswagen Group (Audi, Porsche, Skoda, Volkswagen, Seat). The consequences however have triggered activities within the entire world, within cities, governments and automotive manufacturers. First, a ban of diesel is discussed in cities in order to reduce NO_x emissions as a reaction to the Volkswagen scandal, but also due to weaknesses in the old certification method. Second, the electrification efforts among automotive suppliers have accelerated rapidly since the market reaction on the diesel scandal and NO_x emissions is decreasing diesel sales all over Europe. The timing occurs also at the same time as the CO_2 fleet average requirement is introduced 2021 where diesel played an important part in obtaining lower CO_2 emissions. All these events highlight a very important need: knowledge about control practice and modeling of complex systems, but also that there still are challenges with emissions from spark ignited engines which causes environmental problems. Maybe the most important of all: This time the electric vehicles are here to stay.
I have many people, companies and organizations to thank for making the research possible. As a mechanical engineering student and background within automotive engineering, the support from my supervisor Tomas McKelvey have been very important. Not only the knowledge within the field he has, but also the highly important pedagogical skills. Other important persons that have been involved in discussions have been Niklas Åkerblom, Viktor Larsson and Martin Sivertsson at Volvo Car Corporation. Not only when discussing problems, but also when discussing theory within control practice. I would also like to thank the people providing support for the tests and measurements performed within the scope of the thesis: Markus Ekström at Volvo Car Corporation and Robert Buadu at Chalmers University of Technology. I would also like to thank Volvo Car Corporation for offering the opportunity with the ViPP program where an employee is given the the chance to perform academic research. I am also very proud of Volvo Car Corporation for the efforts in electrification and future company strategy. I would also like to thank Vinnova for providing the funding for this research. Vinnova plays an important role for the technology development and industry competitiveness in Sweden.

Rickard Arvidsson, Gothenburg, February 2018

Contents

1
Introduction

Society is highly dependent on transportation. Economic growth, population growth, higher throughput requirements, globalization and global economies are all factors contributing to transport needs for humans and goods. From 2011 to 2015 the European passenger car fleet grew by 4.5 % from 241 to 252 million vehicles [3]. The passenger car density increases in Europe, from 383 cars per 1000 inhabitants 2011 to 406 cars 2015. The highest motorization rate per 1000 inhabitants in the world can be found in US with 821 vehicles per 1000 inhabitants [3]. The largest increase of passenger cars can be seen in developing countries and China recent years. A decline of passenger vehicles can be seen in US from 2005 to 2015. A large share of the sold vehicles are still driven with fossil fuels [3], [1], [24], [2]. The outlook for electrified vehicle share will be affected by fleet CO_2 requirements in EU. From 2021 the vehicle fleet average for all new cars sold is set to 95 g CO_2/km measured according to the new test method WLTC [23]. In order to meet these targets, the automotive industry is introducing technologies such as mild hybrids (48 V) systems and fully electrified drivetrains or plugin hybrids. One scenario predicts an increase from a 3 % share of fully electrified drivetrains in 2021 to 54 % in 2040 [14]. Other outlooks are more conservative, predicting that full hybrids and electrified vehicles will only account for a 20 % share 2040 [25]. However, the transition will be determined by political decisions, the ability to transform into a clean electricity production, battery technology development and infrastructure investments.

1.1 Air Quality and Greenhouse gases

The industrialization and global wealth is built on fossil fuel dependence. From early industrialization until now the world energy demand have to a large extent been supplied by fossil fuels. According to the world bank, 81 % of the energy need during 2015 was fossil fuel based. Of all the energy produced, 27 % is used by the transport sector. The energy used by the transport sector is either combusted in spark-ignited combustion engines or combusted as jet fuels in gas turbine engines. The combustion process provides work but also produces negative effects such as emissions and CO_2 (Carbon-Dioxide). This makes the transportation sector a significant contributor to anthropogenic CO_2 and pollutants such as CO (Carbon Monoxide), HC/THC (Hydro Carbons / Total Hydo-Carbons), particulate number, particulate matter (PM 2.5, PM 10) and NO_x (Nitrogen Oxides) as a result of the combustion processes. Greenhouse gases and pollutants are contributing to global warming, environmental problems and negative health effects. Smog and high concentrations of NO_x are

also causing local environmental problems in cities. Examples are: Paris, London, Shanghai, Stockholm and Oslo. The EU Air Quality directive allows exceeding 50 $\mu g/m^3$ NO_2 35 days per year. During 2016 in Stuttgart one measurement station reached 87 $\mu g/m^3$ NO_2 in annual mean which is far above the European allowed limit. Measurements in Stockholm during 2011 exceeded a threshold of 60 $\mu g/m^3$ NO_2 during 32 days. From 1990 until 2011 the share of diesel vehicles have increased in EU15 + EFTA countries, from 13.8 % 1990 to 55.7 % 2011 and then again declining from 2011 and forward [24], [1] . Even though an increased share of diesel propelled vehicles have occured, emission levels for NO_x have slightly decreased from $> 40\mu g/m^3$ yearly average in Stockholm down to 10 $\mu g/m^3$ [53]. Overall emissions are also declining. From year 2000 until 2015 the road transport has decreased NO_x with 50 % [22]. Overall a decline in measured city pollution from light duty vehicles can be seen, air quality targets are still highly above the allowed threshold levels for several cities in Europe. Electrification for Hybrids, Plugin Hybrids and Electric cars are contributing to a reduction of local environmental problems and even global CO_2 emissions. A problem with electrified vehicles is still that fossil fuels are to a large extent used for electricity production worldwide. Countries like France, Norway and Sweden have clean electricity, therefore the environmental benefit is higher compared to countries like Poland, Germany and USA. A recent empirical study of electrified vehicles show that PHEV vehicles experience a high utility factor depending on it's electric range. A PHEV with 60 km range utilizes the same annual mileage as an electric vehicle [42]. Considering the benefits from electrified drivetrains, regenerative braking and fossil fuel dependence in the energy sector, the PHEV vehicle with moderate electric range will remain an important technology in the transition to increased transport efficiency and reduced CO_2 emissions. The research will cover optimizing conventional drivetrains, PHEV and PEV drivetrains.

1.2 Legislation and Test Cycles

In the automotive industry, legislation and homologation is used to improve and create common high standards related to safety, quality, environment such as recycleability and in use emissions. Legislation is used as control means for the technology development. In order to compare and regulate fuel consumption and emissions, standardized test cycles are used throughout the world. These are different dependending on market. In US the SFTP(Supplemental Federal Test Procedure) is used containing the standardized FTP (Federal Test Procedure) cycle followed up by two additional tests SC06 and SC03. In EU traditionally NEDC (New European Drive-Cycle, UNECE-R101) has been used until Euro 6 emission levels. NEDC has an average speed of 33 km/h and a maximum acceleration of 1.2 m/s^2. As emissions and fuel consumption requirements have been hardened towards OEM:s an increase in differences between homologation and real driving are highlighted in several publications [21] [39]. The first publications carried out in 2011 demonstrated weaknesses in the existing test method. It was determined that emission limits for real driving highly exceeded the test cycle values [58]. During these tests it was found that average NO_x emissions between Euro 4 and Euro 5 emission standards vehicles for real driving remained unchanged for diesel vehicles and that vehicles

tested in real driving exceeded emission level regulations by a factor 4-7 as an average. The work has resulted in activities leading to a new certification test cycle called WLTP, which is more representative to real driving and includes RDE (Real Driving Emission) in the legislation test procedure. The contribution of this thesis is to focus on actual recorded driving scenarios where predictive data can be used to reduce emissions and fuel consumption under real driving conditions.

Table 1.1: Regulated emission levels and standards for gasoline engines

Emission	Euro 4	Euro 5	Euro 6
CO [g/km]	1.0	1.0	1.0
THC [g/km]	0.1	0.1	0.1
NMHC [g/km]	-	0.068	0.068
NO_x [g/km]	0.08	0.06	0.06
PM [g/km]	-	0.005	0.005
PN [6×10^{12}/km]	-	-	6×10^{11}

1.3 Predictive Information

Predictive information about future driving encorporates different means of information that contains a description of the horizon in front of the vehicle. This includes sensor information, traffic light information, future vehicle speed states, driver classifiers and static information in maps or other statistical data. Information about the road and future ahead enables one to perform optimization of the drivetrain. The potential of using map data was already highlighted in papers [47], [54] for reducing fuel consumption by controlling vehicle speed more efficiently. Intelligent Transport Systems (ITS) became a popular expression in the early 2000:s for means of predictive information and smart infrastructure systems related to traffic light information and vehicles communicating with infrastructure. Predictive information today consists of different means. A map database contains road link information related to geometrical attributes such as curve radius, road slope, altitude information and road sign speed. Another source of information is radar and lidar (Light Detection and Ranging), which can be used to predict the future velocity for a short distance in front of the vehicle. A more recent area is statistical models which provide predictive information based on the usage of statistical models.

1.3.1 Map Data

Map data is an important source in terms of representing geometrical attributes along the vehicle's most probable future path. ADAS (Advanced Driver Assistance System) was mentioned already in [15], but the first applications using map information was published a few years later [50]. The focus has until now been to utilize map information to improve safety of the vehicles. Today the map data is useful for cruise controllers where curve speed radius is used to limit lateral acceleration at turning with deceleration before the curve [31], [44]. The cruise control together with altitude data can also control vehicle speed towards improved comfort. Later

publications have focused on publishing methods using techniques from [47] together with map data in order to improve real driving emissions and real fuel consumption [29], [37]. This can be achieved by controlling drivetrain actuators and speed of the vehicle by using map data as an input. Many methods practiced can provide fuel consumption benefits but varies depending on robustness towards disturbance factors [5], [7]. Inaccurate map-data and ill-positioned slopes is one common disturbance factor.

1.3.2 Sensor Measurements

Traditionally cruise controllers worked without sensor information other than the measured vehicle speed, controlling the propulsive torque to meet a set speed. Functions like adaptive cruise control uses radar and lidar to measure distance and reference speed to objects and adapt the following car speed to the target vehicle speed. An example can be seen in Figure 1.1 below.

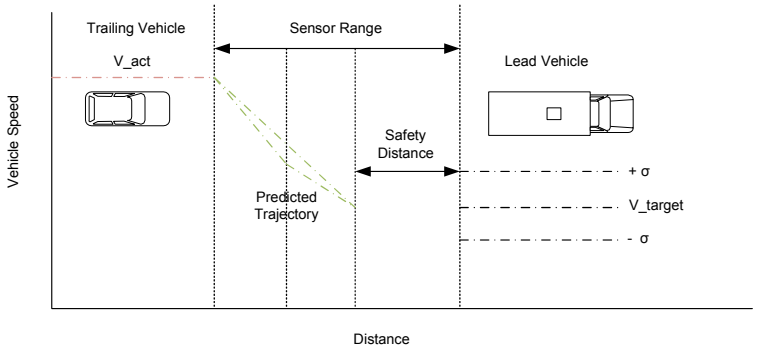

Figure 1.1: A trailing vehicle with distance measurements to a followed vehicle with predicted speed trajectory

Together with other external information an optimal speed trajectory could be calculated [31], [45]. That is: calculating the optimum gap within the safety margins to the following vehicle in order to select the best gears and optimize operating point of the combustion engine. A study of both braking and acceleration responses with following vehicles have been done which highlighted the influence of reference tracking ability when system response is derated at for instance shifting sequences [4]. Merging maneuvers have been studied separately where a optimum merge can be found for trucks given a certain distance which reduces energy consumption [33]. The other problem as shown in Figure 1.1 is to compute the best transitions to a lower vehicle speed including different possible decisions such as engine off, idle coast (in neutral gear) or for a vehicle with regeneration possibilities to perform regenerative braking for passenger cars. The vehicle speed trajectory appear different if the control objective allows idle control or engine off transitions or if the vehicle is propelled with an electrical motor or a combustion engine.

1.3.3 Data Driven Statistical Models

Route historical data can be stored for individual vehicles and be used for data models in the vehicle. This can incorporate statistical traffic models of traffic flows at different times or energy related data to the vehicle's energy consumption throughout the driving. Studies have been carried out analyzing speed prediction modeling to the road segments using a DPGMM (Dirichlet Process Gaussian Mixture Model). Given a certain road segment and time window it is assumed that the measured velocities and other parametric measures (energy consumption) follow a mixture distribution depending on various components. Affecting components are weather conditions, road conditions, driver behavior or vehicle specific conditions.

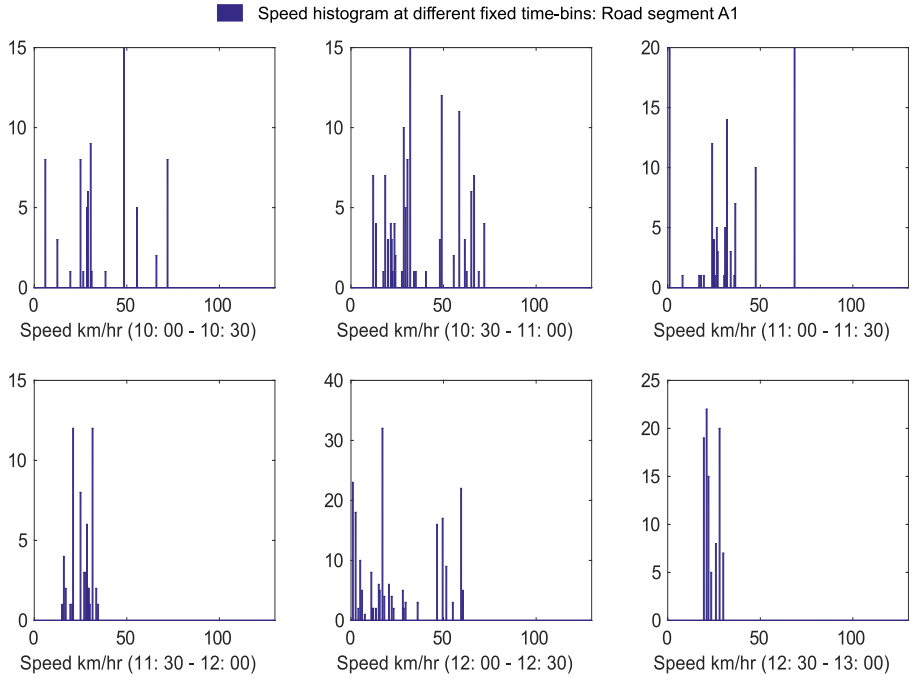

Figure 1.2: Distribution of vehicle speed collected for several vehicles at a given road segment. Shown is the vehicle speed bins on x-axis and number of observations on y-axis

A typical speed distribution of a road segment can be seen in Figure 1.2 divided into a 30 minute time interval. The data is collected from road segments in Gothenburg from three individual test vehicles. Statistical models can also be used to predict energy consumption or speed on road segments, several mentioned in [13], [8]. Implemented functions so far in the automotive industry have usually been offline classification of driver behaviour. Thereafter rule based criteria based on the sampled observations of driver type are adjusting the shift points after the driver type [59].

1.4 Objectives

The thesis is based on the objective that predictive information can be used to improve drivetrain efficiency and emissions for SI operated drivetrains and hybrid drivetrains or increasing electric range for electrified vehicles. The work applies established optimization methods to problems in an automotive context. The results are evaluated for the methods by simple simulation models, full vehicle simulation models and real tests on physical objects in test rigs. Several problems arise when the methods are applied in a physical object, one is the map data and information containing future path description which is approximated and may include errors or disturbances. Another is the driver intention, which is not always known. Therefore, uncertainties in the prediction needs to be taken into consideration when the methods are applied.

2
Modeling and Methods

The following chapter starts with briefly describing the longitudinal motion of the vehicle with resistance forces. Thereafter a description of each component of the drivetrain is described: Combustion engine with the different aspects considered in a SI engine, high voltage battery and transmission. Finally a description of the control and optimization methods follows.

2.1 Drivetrain Modeling

The vehicle longitudinal motion is divided into two separate components. The resistive force containing slope, acceleration, rolling resistance and aerodynamic drag resistance. The propelling forces consists of inertia with dynamics and combustion engine or electrical machine. We denote vehicle acceleration as $\dot{v}$. The vehicle rolling resistance force F_r is a function of f_0 [-] and f_1 $[\frac{1}{m/s}]$. The vehicle drag resistance force is a function of f_2 $[\frac{1}{(m/s)^2}]$.

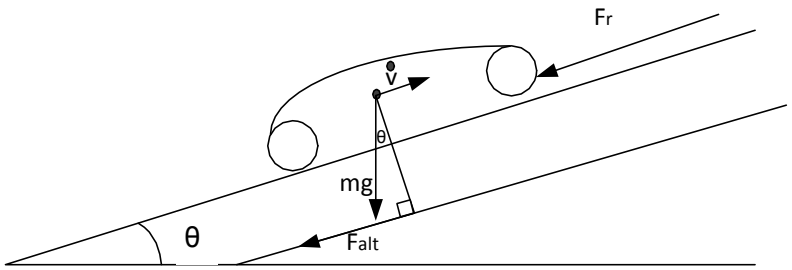

Figure 2.1: Longitudinal vehicle model: F_r denotes the resistance forces caused by air and drag, F_{alt} is the force related to the slope and mass, θ is the slope

The simplified road load resistance force model along the longitudinal axis x is governed by

$$\sum F_x = \frac{-T_w}{r_w} - m\dot{v} + f_0 + f_1 v\cos\theta + f_2 v^2 + mg\sin\theta \tag{2.1}$$

The wheel torque is denoted by T_w which is the shaft torque on front and rear shaft transferred to the road, wheel radius is denoted r_w. It contains the vehicular motion equation, rolling resistance force, aerodynamic drag force and gravity force.

The simplified road load force model along the longitudinal axis x is governed by Equation 2.1. The wheel torque contains inertia of the drivetrain and the propelling motor where the losses of the transmission is subtracted. The relationship between the wheel torque and the propulsion source can be seen in Figure 2.2. Here we assume that the drive-shafts have infinite stiffness and that torque transfer over the tire to the road is ideal with zero slip, meaning that tire losses are included in the rolling resistance coefficient f_1 and independent on torque transferred.

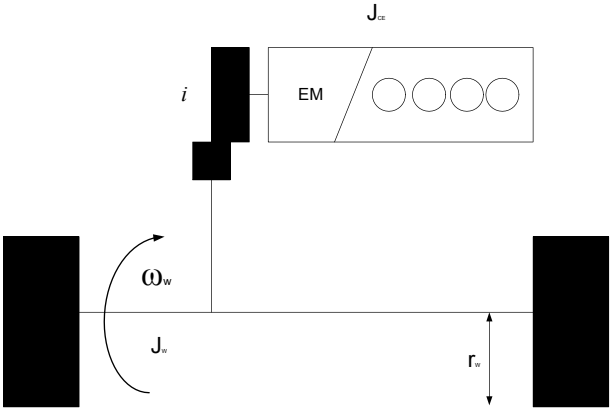

Figure 2.2: Representing torque distribution from torque source to the wheels including the mechanical system. Wheel radius is denoted with r_w.

Consider again Figure 2.2. We denote the gear ratio as i and the inertia J. When the wheel slip is zero we can consider the wheel torque T_w to be equivalent to Equation 2.2. We write the torque transfer to the wheels as a function of the mechanical system and the propelling forces according to:

$$T_w = T_{ce}i + J_{ce}\dot{\omega}_w i^2 + J_w\dot{\omega}_w \tag{2.2}$$

The rotational speed on the shaft ω_w is proportional to the vehicle speed in Equation 2.1 when the slip is small or close to zero we have: $v = \omega_w r_w$ and therefore $\dot{v} = \dot{\omega}_w r_w$. T_{ce} above can denote both electrical machine torque and combustion engine braking torque.

2.1.1 Gearbox and Converter

The torque balance between the propulsion source T_{ce} and T_w is described in 2.2. The gearbox considered is a planetary gearbox with converter. Important components in the converter consists of an impeller, turbine and a lock-up clutch. When the engine is running at idle speed and the vehicle is stationary, engine speed is synchronized with impeller and the turbine is stalled. The parallel hybrid studied contains combustion engine and an electrical machine in front where the electric machine is mounted on the crankshaft. We define two different modes for the automatic gearbox: Lock-up with synchronized speed and engine speed slip over the torque converter (torque conversion). During the lock-up mode the engine speed is

fixed towards the input shaft speed thus torque transfer is described by:

$$T_w = \Big\{(T_{ce} + T_{em})i + (J_{ce} + J_{em})\dot{\omega}_w i^2\Big\}\eta_{gb} + J_w\dot{\omega}_w \tag{2.3}$$

The efficiency of the gearbox is significantly dependent on the gearbox temperature due to differences in oil viscosity and friction, but also tolerances within the gearbox that are affected by increased temperature. The gearbox efficiency, η_{gb} is a function of the gear ratio, input shaft torque and rotational speed of the output shaft. During the torque conversion state the power capacity of the engine is used to convert to a higher torque. Speed ratio is the difference between the engine speed and the output shaft speed that is used to describe the torque ratio (torque increase possible) between the crankshaft and input shaft. We denote the torque ratio γ_r. The transferred wheel torque is then described as:

$$T_w = \gamma_r(\frac{\omega_w i}{\omega_{ce}})\Big\{(T_{ce} + T_{em})i + (J_{ce} + J_{em})\dot{\omega}_{ce} i^2\Big\}\eta_{gb} + J_w\dot{\omega}_w \tag{2.4}$$

The torque ratio γ_r is dependent on torque direction. During positive torque transfer from the engine the impeller drives the oil pressure and rotates the turbine. At engine braking this negative torque transfer, the turbine in the converter drives the impeller. The most significant factor affecting the torque ratio is the speed ratio between the impeller and turbine.

2.1.2 Combustion Engine Modeling

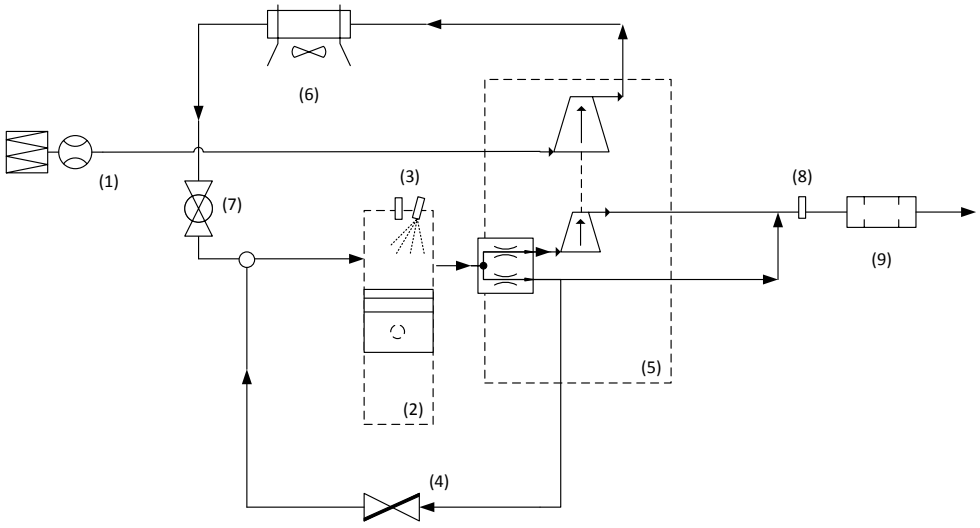

Figure 2.3: Schematic overview of the engine and it's components. Components shown are 1) MAF (mass air flow sensor), 2) Combustion chamber, 3) Spark system and fuel Injector, 4) EGR (exhaust gas re-circulation valve), 5) Turbo, compressor and wastegate, 6) Intercooler, 7) Throttle 8) Oxygen sensor and 9) Exhaust after treatment system.

The combustion engine is a highly non-linear system containing physical processes that requires high computational effort to model, such as air flow and air response,

fuel and air vapor mixture, vaporization, flame propagation and reaction kinetics. A schematic overview of the gasoline engine system can be seen in Figure 2.3 . Engine response and air kinetics is highly dependent on compressed air from the turbo. The air input mass flow is measured with the mass air flow meter. Fuel spray is injected in the combustion chamber and ignited with the spark system (if not stratified charge compression ignition is used). Oxygen concentration is measured after the combustion through an oxygen sensor and emissions are further reduced in the aftertreatment system, which is a three-way catalyst.
The four stroke cycle is visualized in Figure 2.4, illustrating the pump work for a combustion engine. Measurements are carried out at lean $\lambda = 1.45$ compared to stoichiometric $\lambda = 1.00$.

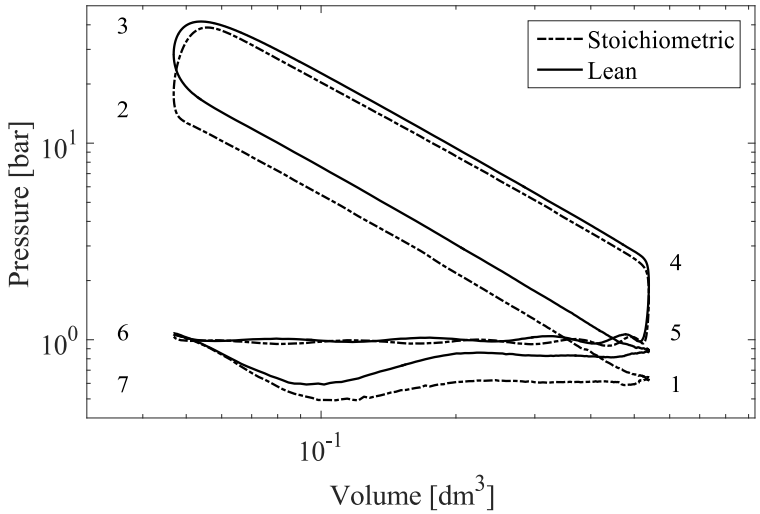

Figure 2.4: P-V diagram of the engine measured at lean and stoichiometric conditions. Measurements are done on a similar engine used in this work from [20].

The ideal otto cycle can be described with the following steps:
1 - 2: Isentropic compression
2 - 3: Constant volume heat addition
3 - 4: Isentropic expansion
4 - 1: Constant volume heat rejection
Pump losses in the four-stroke otto cycle are spanned by: 5, 6, 7, 1. In Figure 2.4 it can be seen that the pump losses for lean combustion are smaller than the losses for stoichiometric combustion.

2.1.2.1 Fuel Consumption

An approximation of the engine fuel consumption can be taken from steady state operating point measurements in a BSFC (Brake Specific Fuel Consumption) map. In Figure 2.5 a BSFC map is shown and we notice that the best efficiency is obtained at 2500 rpm and 180 Nm.

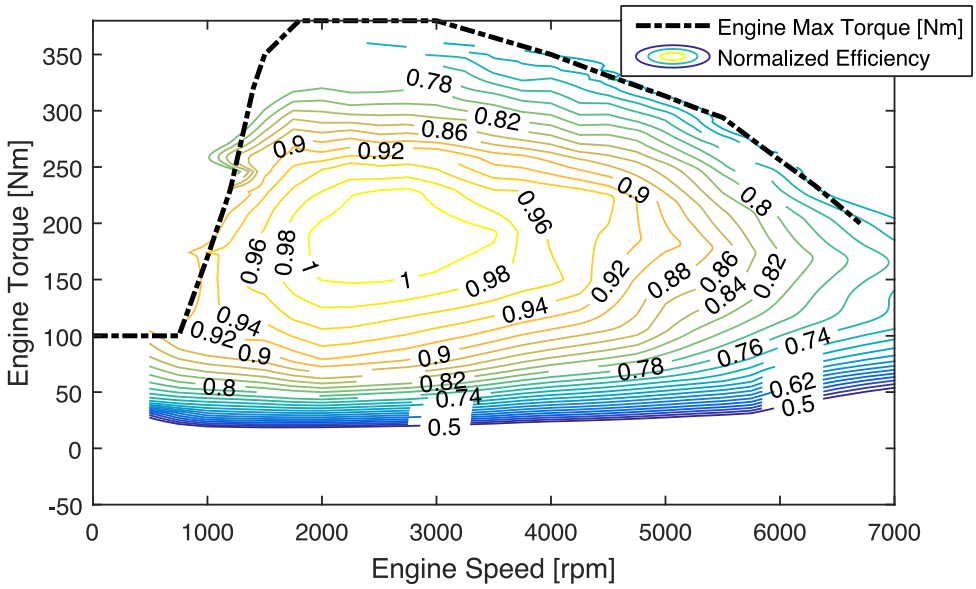

Figure 2.5: Normalized BSFC map to determine fuel consumption cost and maximum engine torque. The best efficiency is obtained at the contour with value 1, which accounts for the highest efficiency.

There exists several challenges with a BSFC modelling approach. The mapping is carried out at maximum brake torque which simplified is the maximum spark advance with knock constraints and problems may arise when using BSFC as cost estimation in transient drivecycles. During transient driving or shifting gears, deviation from maximum spark advance is necessary in order to to maintain drivability [18], [34], [32]. Other modeling errors from BSFC consumption models are errors propagating from engine power changes. At fast transients: usually aggressive throttle opening is applied not only affecting deviations in spark advance strategy but also intake and exhaust cam phasing. In order to compensate for the steady state deviations in fuel consumption modeling different transient compensation factors can be added [34], [32], [18].

2.1.2.2 Emissions

Emission formation occurs during different operating modes in the engine. Static mapped emissions are typically due to several effects mentioned in [28]. Unburned fuel-air mixture causes HC after the combustion process, either wall film or residuals from partial burning or complete misfire. This can also occur in transients when air to fuel ratio, EGR and spark timing control causes combustion instability. CO emissions are mainly controlled by air to fuel ratio. A SI engine is normally operated in stoichiometric conditions. At stoichiometric conditions the Air-fuel ratio is 14.7:1, which describes air mass compared to fuel quantity mass. During stoichiometric conditions $\lambda = 1.00$, the engine out CO emissions drops to low values and catalyst aftertreatment system have high conversion efficiency. We define λ as

$$\lambda = \frac{A/F}{(A/F)_{stoich}} \tag{2.5}$$

Lean combustion for SI petrol engines have several positive effects such as reduced pump work and higher combustion efficiency [20]. However lean combustion also introduces a higher rate of NO_x formation and a three way catalyst is not able to reduce NO_x due to excess air in the catalyst [43], [20]. Therefore emission models and catalyst states (such as oxygen storage) levels will be important in the combustion engine control in the nearby future.

2.1.2.3 Spark Advance

For a SI engine, the timing of a spark event is known as spark advance. The spark advance is used to obtain highest efficiency during the combustion. An optimized ignition results in the Maximum Brake Torque (MBT) from the engine [48]. Ignition can be retarded instantaneously by spark advance controllers. One example is knock feedback control to retard ignition. Knock is an effect caused by high temperatures inside the cylinder, hardware design, cylinder pressure and other aspects. The fuel-air mix is pre-ignited close to hot surfaces and high pressures. This phenomena causes high peak pressure inside the cylinder which causes undesirable wear of components and increased NO_x, emissions [35], [40]. It is a phenomena challenging in downsized engines with increased compression ratio and EGR which imposes a risk of knock at high load conditions.

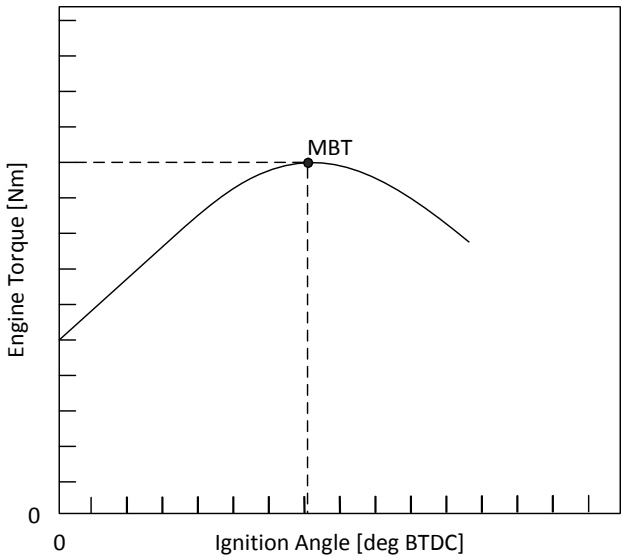

Figure 2.6: Representing maximum brake torque for a SI engine and advanced spark angle.

Spark advance is calibrated such that the engine achieves it's maximum thermal efficiency that avoids knock and combustion instability. Thermal efficiency is defined as the indicated work on piston at one cycle compared to the injected fuel energy. The work performed is simply defined as $W_i = \int p \mathrm{d}V$ where p is the cylinder pressure and $\mathrm{d}V$ is the differential of cylinder volume. The combustion phase (crank angle after TDC of 50 % burned) is affected by spark advance. Knock probability, knock

intensity mean and variance increases with advancing CA50 [51] . When increasing λ to lean combustion the combustion process will become slower, slower heat release process which affects the knock density.

2.1.2.4 Air Dynamics

Air dynamics summarizes the air flow to the cylinders which is affected by the throttle pressure drop, boost pressure and engine volumetric efficiency. Air dynamics is highly affecting the engine response and is one of the significant limitations for engine torque capability. The mass flow into the cylinder $\dot{m}_{ac}$ is given by the ideal gas law, $PV = nRT$ where P is the pressure, V is the gas volume, n is the gas amount in moles, R and T are the ideal gas constant and absolute gas temperature respectively. We introduce a pressure drop coefficient depending on the throttle angle and pressure η_{vol} and consider the engine displacement volume and engine speed. The mass air flow determined from the ideal gas law can then be written as

$$\dot{m}_{ac} = \eta_{vol}(n_e, p_{im}, ...)\frac{V_d n_{CE} p_{im}}{n_r R T_{im}} \tag{2.6}$$

and

$$\eta_{vol} = c_0 + c_1\sqrt{p_{im}} + c_2\sqrt{n_{CE}}$$

is the approximated volumetric efficiency. V_d is the displacement volume, T_{im} is the intake manifold temperature and p_{im} is the intake manifold pressure. Number of revolutions per cycle is denoted n_r. Clearly the torque delivered by the engine is strictly depending on the engine speed and intake manifold pressure.

2.1.3 Battery Modeling

Electrified propulsion powertrains have voltage levels varying from 12 V and upwards. Typically higher power outputs requires higher voltage levels in order to reduce electrical losses. Toyota Prius have a nominal voltage of 202.6 V. The batteries covered in the thesis considers voltage levels above 300 V. Common methods to describe battery characteristics are to use standardized discharge tests to determine battery parameters [17], [56], [12]. The single resistive circuit model lacks accuracy in modeling DC voltage transients [6]. Figure 2.7 shows an resistive capacitive equivalent circuit of a battery. Batteries can also be described with electrochemical models [57] .

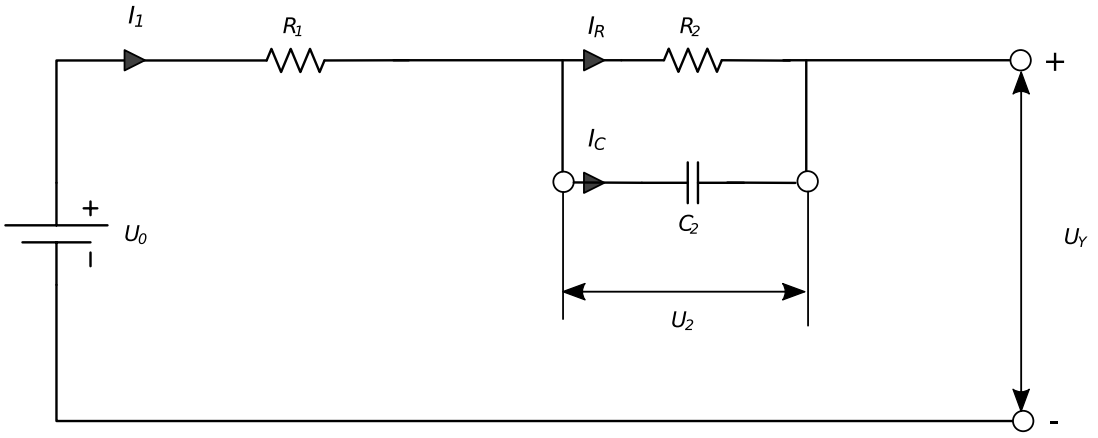

Figure 2.7: Representing a RC circuit equivalent battery model.

A battery voltage model including an RC circuit is illustrated in Figure 2.7. The voltage U_y can be described as:

$$U_y = U_0 - R_1 I_1 - U_2 \tag{2.7}$$

where U_2 is representing the voltage drop over the capacitance. The state equation is written as

$$\begin{bmatrix} \dot{U}_2 \\ U_y \end{bmatrix} = \begin{bmatrix} \frac{-1}{R_2 C_2} \\ -1 \end{bmatrix} U_2 + \begin{bmatrix} 0 \\ 1 \end{bmatrix} U_0 + \begin{bmatrix} \frac{1}{C_2} \\ -R_1 \end{bmatrix} I_1 \tag{2.8}$$

The resistances are dependent on state of charge and temperature. Open circuit voltage U_0 is mainly depending on state of charge. In general battery losses increase with decreasing state of charge and decreasing temperature. We denote the nominal charge in the cell as Q_{nom} which is the charge capacity at 100 % SOC. In general state of charge is expressed as

$$\dot{SOC} = \frac{-I_1}{Q_{nom}} \tag{2.9}$$

P_b is the delivered battery power or the resulting DC equivalent charging power. Usually U_y and I_1 are measured quantities in the vehicle from where state of charge level is estimated. Simplified battery losses can be determined by $P_{loss} \approx I_1^2 R_1$ or estimated by parameter estimation from $P_{loss} = (U_0 - U_y) I_1$ where U_0 is an estimated parameter and U_y and I_1 measured.

2.2 Optimization Methods

The optimal control problem we aim to solve is to find the sequence of controls that minimizes the fuel mass used at a given route or part of a route. We consider a route with a time $0 \leq t \leq t_f$. For a conventional drivetrain this can be summarized as minimizing the cost function

$$J = \int_0^{t_f} \dot{m}_f(T_{ce}(t), \omega(t)) dt \tag{2.10}$$

where T_{ce} [Nm] and $\omega_{ce}(t)$ [rad/s] is the torque and speed of the combustion engine. $\dot{m}_f$ is the instantaneous fuel consumption. Depending on the drivetrain context this can be done by selecting a set of control sequences $u(t)$ for instance gears and electric motor torque such that the states $x(t)$ e.g. battery charge level, engine speed and vehicle speed remains within the constrained limits.

2.2.1 Model Predictive Control

Model Predictive Control (MPC) is a method used to optimize a cost for a dynamical system with a given horizon. The benefit of MPC is that it is capable of handling constraints. In general a model is used to predict the future output and optimize the control signal with an objective to minimize a cost. The problems that are studied for optimizing efficiency and emissions for drivetrains are typically finite horizon of N steps due to the unpredictable circumstances. Optimizing the usage of energy resources to a final destination can also be considered as a finite horizon problem over a longer distance. We consider the discrete time non-linear system defined in 2.1 as $x_{t+1} = f(x(t), u(t))$ where $x \in \mathbb{R}^n$ is the state vector and $u \in \mathbb{R}^m$ is the control input. In the above formulation we consider the vehicle speed as the state x and control signal u is the power applied to the wheels. We denote the position in the drivecycle as $\int_{t_0}^{t_f} x(t)dt$. The engine BSFC map can be approximated as a quadratic cost. The general MPC quadratic cost formulation can be written as

$$J(x_0, U_0) = x'_N P x_N + \sum_{k=0}^{N-1} x'_k Q x_k + u'_k R u_k \tag{2.11}$$

where P, Q and R are matrices used for the cost function to preserve final state, reference tracking and control signal cost, referring to power needed to move the vehicle. The solution can be obtained using dynamic programming as described below or a quadratic program solver.

2.2.2 ECMS

Analytical solutions can be used for solving optimization problems, a method used is Equivalent Consumption Minimization Strategy (ECMS). ECMS can be stated as following: For each time $0 \leq t \leq t_f$ an equivalence factor or co-state λ_k, $k = 1, 2, ...n$ is used to balance cost between a cost function dependent on different means [58], [49], [41]. Such a problem is to provide an optimal torque split balance between electric motor torque and combustion engine torque. Another example considered is to balance vehicle speed towards travelling time [46]. We define the generic cost formulation as

$$J(t) = \int_0^{t_f} g(x(t), u(t)) + \lambda(t) f(x(t), u(t)) dt \tag{2.12}$$

where $g(x(t), u(t))$ is the cost function and $f(x(t), u(t))$ is the state equation. Consider the cost to be the fuel mass $\dot{m}_f$ and the system state $x(t)$ as SOC. Then the control signals $u(t)$ are the engine torque and battery current. We assume that the transfer function is known from engine torque to battery current and that we study

a series hybrid from Paper III. From Equation (2.9) it is given that change in SOC is depending on current from the battery. Only studying the aspect of the co-state from the Hamiltonian, it is clear that $\dot{\lambda}$ can be derived as

$$\dot{\lambda} = -\lambda \frac{100}{Q_{nom}} \frac{\mathrm{d}I_1}{\mathrm{d}U_0} \frac{\mathrm{d}U_0}{\mathrm{d}SOC} \tag{2.13}$$

where Q_{nom} is the nominal charge capacity of the battery pack. Important property of the co-state is: If $\frac{\mathrm{d}U_0}{\mathrm{d}SOC} \approx 0$ then the co-state remains constant. This is applicable if changes in SOC are small. It is known that the current is directly depending on the state of charge level, since decreasing open circuit voltage at lower state of charge demands higher current output and thus also more rapid SOC degradation. ECMS will be further studied in future work for torque split applications where battery SOC can be considered constant.

2.2.3 Dynamic Programming

Dynamic programming (DP) is an approximate recursive approach which uses the principle of optimality, [9], [11]. The principle of optimality holds: An optimal path or policy has the property that independent of initial states and control decisions, the remaining control decisions must constitute an optimal policy with regard to the states resulting from the first control decisions [10]. In order for the optimal path to hold, it requires that the states are not depending on its previous states (Markov property). We define the the problem with decision points or segments $k \in \mathcal{K}$, a set of states $x \in \mathcal{X}$ and control signals $u \in \mathcal{U}$. The general discrete time optimal control problem can be formulated as

$$J^* = \min_{u_k} \Big\{ \sum_{k=1}^{N-1} g(u_k, x_k) \Big\} \tag{2.14}$$

$$\text{s.t}$$

$$x_{k+1} = f(u_k, x_k)$$

$$x_k \in \mathcal{X}_k, u_k \in \mathcal{U}_k$$

where $\mathcal{X}_k$ and $\mathcal{U}_k$ are the sets of feasible states and inputs respectively. We denote the cost function $g(u_k, x_k)$. The problem in Equation 2.14 is numerically solved using DP [16], discretizing the state space into a finite set. The solution provided is a approximated solution to the problem in Equation 2.14. The finite set contains states inside and outside the desirable state set to allow cost interpolation close to the edge state for the case implicit dynamic programming described below. Figure 2.8 shows a graph representation of the state and control propagation. Since Markov property holds, the network can be calculated both forward from x_0 to x_N or backward from x_N to x_0.

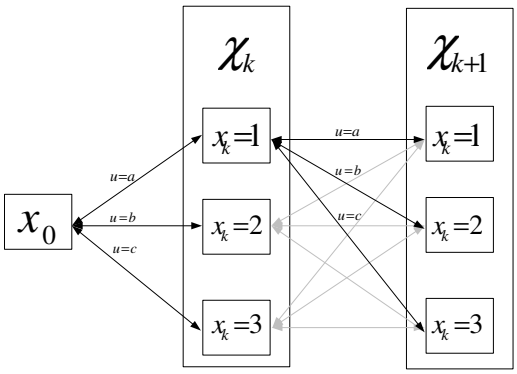

Figure 2.8: Graph representation of the DP problem. The control $u_k \in \mathcal{U}$ are the feasible controls that lead to $\mathcal{X}_{k+1}$.

In the case where explicit dynamic programming can be applied, the need for including states outside the desirable state set is not needed. Efficient and common algorithms like Dijkstra [19] works for shortest path problems with a positive defined cost and can be used for combustion engine and gear optimization. For hybrid and electric vehicles that may benefit from downhill driving and braking introduce a negative cost since energy be produced, therefore Dijkstra is not suitable for solving such problems. We divide the DP problem into two different unique cases for how states and control signals have been used in the thesis. Method 1 is used together with the existing vehicle software and is running with a recommended set point for a high level controller. The actuator demand is delegated to a local controller which provides the coordination between the high level controller and the local controller. Method 2 is used directly with a model of the state transition and determines the control signal explicitly.

2.2.3.1 Method 1: Implicit DP

Method 1 describes the special case with discretized control signals in fixed segments simulated in continuous time. Here, each discretized segment contains a time subset for which each simulation is performed. The state output however cannot explicitly be determined since the model contain hidden states in an existing controller structure external dependencies from the vehicle software. Therefore, applying interpolation for the state and cost output is necessary. The general implicit DP formulation can be stated as

$$J^* = \min_{u_k} \Big\{ \sum_{k=1}^{N-1} \int_{t_k}^{t_{k+1}} g(u_k, x(t)) dt \Big\} \tag{2.15}$$

s.t

$$\dot{x}(t) = f(u_k, x(t)), \quad t_k \leq t < t_{k+1}$$

$$x(t) \in \mathcal{X}_k, u_k \in \mathcal{U}_k$$

One important property is that the control signal u_k remains constant during $t_k \leq t < t_{k+1}$. Initialization of states are carried out such that $x(t_k) = x_k$ for forward propagation.

2.2.3.2 Method 2: Explicit DP

In Method 2 the control signal is given from from the state transitions and the system dynamics. If u is a set of discretized feasible control inputs $\in \mathcal{U}_{\|}$, a state transition is called feasible if there exist one control input u_k such that $x_k \rightarrow x_{k+1}$. One example is the input torque provided by Equation 2.1 and feasibility with Equation 2.2. The general explicit DP problem can be defined as

$$J^* = \min_{u_k} \Big\{ \sum_{k=1}^{N-1} g(u_k, \omega_k) \Big\} \tag{2.16}$$

$$\text{s.t}$$

$$x_{k+1} = f(x_k, u_k)$$

$$x_k \in \mathcal{X}_k, u_k \in \mathcal{U}_k$$

where the states x_k are discrete and the control signals are $u_k \in \mathcal{U}_{\|}$ are continuous in the interval $u_{min} \leq u_k \leq u_{max}$. Any state transition leading to a control policy outside the interval of u is considered as an unfeasible state transition.

3

Test Setup

This chapter summarizes the test and evaluation methods used within the scope of the thesis. Evaluation has been carried using computer models and rig tests at Chalmers University of Technology and Emission test lab at Volvo Car Corporation.

3.1 Dynamometer Tests

The rig test equipment contains four chassis dynamometers simulating road load for the test cycles according to 2.1. The driver controller is included in the rig system and is modeled as a PI speed controller with vehicle speed look-ahead, close to target speed a reduced gain ensures stability at constant speed. Figure 5.1 shows a vehicle installed in the test rig used for the testing conducted.

Figure 3.1: Test object installed in the test rig. Dynamometers attached to the wheels front and rear

3.1.1 Fuel Consumption Measurements

Fuel consumption is measured and calculated with two different methods. First method uses an injector flow estimation model based on the fuel pressure (high pressure side) sensor. The fuel flow is then calculated in the engine ECU from the pressure and injector duty cycle. Method 2 uses an external fuel mass flow meter connected to the feed to the high pressure fuel pump (by-passing the vehicle fuel tank). The flow measurement device is not related to the vehicle control system. The external fuel-flow measurement is sampled with a frequency of 20 Hz. The device measures fuel flow during stationary conditions and transients according to ISO-16183 [30].

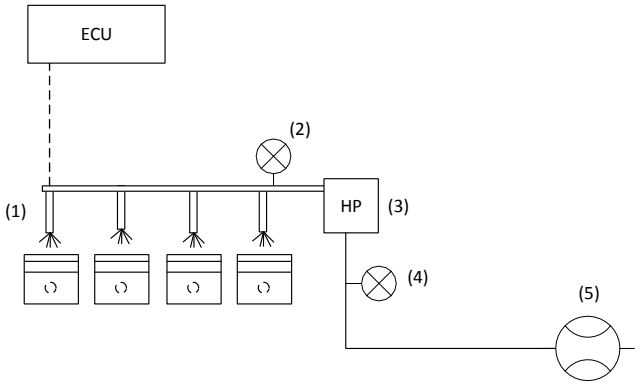

Figure 3.2: Schematic overview of sensors and measurements in the test-rig. The components are: (1) injectors, (2) high pressure fuel sensor, (3) high pressure fuel pump, (4) low pressure sensor and (5) external fuel flow measurement

A comparison of method 1 where the fuel flow is calculated by the engine ECU and method 2 (ISO-16183) can be seen in Figure 3.3. A comparison is carried out in a drivecycle with stationary and transient conditions under a 48 second interval. The fuel mass flow for the two methods is integrated over time and the comparison is done for the accumulated value for the entire drivecycle. The overall fuel mass peak norm-difference between the methods is measured to be less than 0.4 % for all 21 test series conducted and average error 0.1 %.

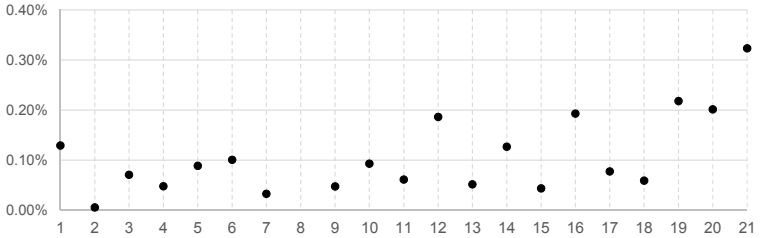

Figure 3.3: Comparison between fuel consumption measurement methods for one drive-cycle. X-axis represents each test in randomized order and absolute difference in estimated fuel mass on the Y-axis.

3.2 Emission Measurements

Emissions are measured with a FTIR (Fourier-transform infrared spectroscopy) measurement system [26], [52]. A emissions sample is measured with a beam of infrared light is passed through. The energy absorbed at each wavelength is used to create an absorbance spectrum for the sample whereas a result of fraction or concentration is obtained. In order to calculate mass equivalent emissions per kilometer. First exhaust mass flow can be measured with an exhaust flow meter (EFM). Exhaust flow can also be estimated by the injected fuel mass which is known (with an average error of 0.1 % as seen in Figure 3.3) and measured inlet air. The air flow is measured with an mass air flow (MAF) sensor and pressure drop over the throttle is measured with an intake pressure sensor. Together with the intake pressure intake temperature measurements, the air mass can be calculated with Equation (2.6) at each sampled instance. The exhaust mass flow is then determined according to:

$$m_{exh} = (m_{MAF} + m_{fuel}) \tag{3.1}$$

3.3 Full Vehicle Simulation

A full vehicle model where drivetrain, auxiliary components, wheels and chassis are modeled is used for the optimization. The tool used is based on Matlab Simulink and is called VSIM (Volvo Car Simulation Toolbox) and contains a full drivetrain model of the vehicle. The dynamics covering rotational inertia and friction losses are modeled in plant models solved using an ordinary ODE45 solver. An overview of the simulation setup can be seen in Figure 3.4.

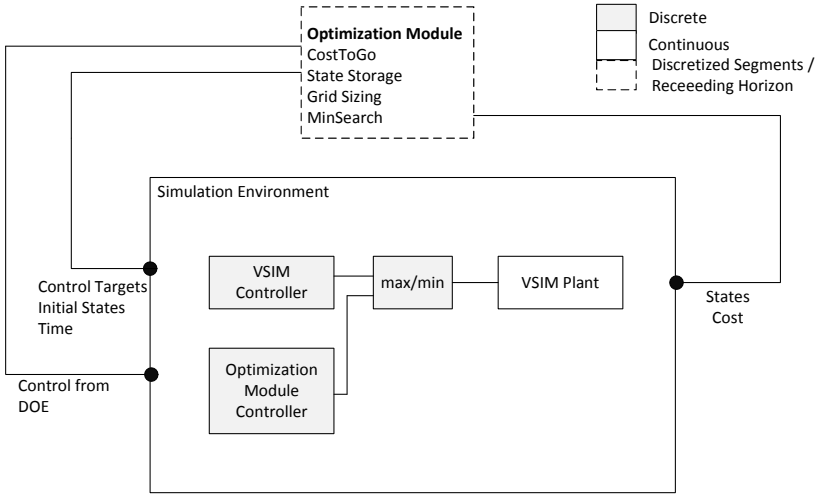

Figure 3.4: Representing the simulation setup environment and optimization environment

The VSIM controller model is scheduled in discrete time similar as the vehicle ECU. The control signals are engine state (on/off), torque to each actuator or gear decision depending on requested wheel torque and vehicle speed. The applied signals are constant for each segment or pre-calculated cost factors using ECMS. The optimization module divides the drivecycle and state-space into small segments and a state grid. The model is then modeled in continuous time. Dividing drive-cycle between the discrete segments is carried out by the optimization module and the initial states are given by the state grid. Cost and states are calculated from the continuous time simulation model and interpolated to fit the state grid. The plant provides an internal feedback loop of the states during the simulations to the conventional rule based controller and look-ahead controller. A switching module provides the coordination between the conventional rule based controller and the look-ahead controller (max/min) in Figure 3.4, such that feasibility and operationable limits are always fulfilled.

4
Results

This chapter summarizes the main results obtained within the scope of the research. Published papers are summarized in Section 4.1. The work began in conducting simulation studies that was compared to rig-tests. It was soon discovered that engine start occurrences in the rig tests differed from the simulation model. The reason was found to be differences in voltage drop during transients for the high voltage battery. The voltage drop in the rig tests was higher than in the simulation model. This had a direct impact on the engine start occurrences for the rig tests for which occurred at different times in the drivecycle compared to the simulation model. A method to sample battery data from CAN measurements in the vehicle (Controller Area Network) and parameterize a battery model structure offline was developed in Paper I. Different model complexity structures was evaluated towards battery output voltage accuracy.
The work continued in Paper II evaluating fuel consumption for different high level engine state controllers during a route comparing optimization and modeling approaches. The rate of discharging the battery was optimized to minimize fuel consumption. Optimization strategies was calculated offline in simulation models with findings from Paper I. The offline calculated parameters were integrated to the vehicle ECU and tested for a realistic drivecycle with different drivers for a parallel hybrid drivetrain.
Paper III is a continuation of Paper II that includes more aspects of discharge rates and investigates how the engine operating points and speed dynamics are affected by SOC over a drivecycle applied for a series hybrid. The most significant difference from Paper II is that when the engine is running, shift points are not statically defined and decided. Instead any operating point and speed is possible for the combustion engine. This not only includes more states and control decisions, but also takes more time to solve. The number of states and control decision variables were compared for the engine at the same time the optimal discharge rate was found.

4.1 Published Papers

Paper I

Three different battery models with different model complexity have been evaluated. Current and voltage is collected during real driving in a plugin hybrid and tested to fit measured voltage towards a modeled voltage output. The battery is modeled as equivalent linear electric circuits. A resistive circuit is compared to a RC circuit and

a dual RC circuit. The test data used for battery parameter classification is recorded mainly at very low C-rates and at state of charge levels close to charge sustain level (25 %). The temperature of the cells in the training data varied from 5 degrees C to 23 degrees C. It was found during the study that the modeling complexity affected the result for voltage goodness of fit. The single resistance battery model could not represent voltage dynamics during current step changes. The best result was obtained by using a resistance in series with a resistance and capacitance (RC). The average goodness of fit for the R circuit of 70 %. Best result towards the training data was obtained by the single RC circuit model with an average of 97 % goodness of fit. The dual RC circuit model did not represent a normally distributed fit towards the training data. The reason for the less accurate model fit for dual RC circuit was not a part of the Paper, however a probable reason is that longer discharge pulses were not present in the training data sampled from the real driving that is available in the standardized HPPC test-cycle.

Paper II

The Paper compares different control methods to discharge a high voltage battery in a parallel plugin hybrid electric vehicle. The control methods are compared to a conventional depletion-sustain strategy without any look-ahead information. First a DP method is used to determine a lookup table of driver demanded power requests for which engine start occurs. The power request map is a grid in distance and SOC. This is compared to a look-ahead heuristic strategy that estimates each segment energy usage based on a road load model and vehicle model. Thereafter the algorithms portions the electric drive into low average power segments. In the DP algorithm the state feedback was SOC at a given distance in the cycle with a pre-calculated lookup-table for engine start power request. In the heuristic method: the SOC trajectory was obtained from the sorting algorithm and the engine on requested power was handled by a conventional SOC P-controller. The results from the simulations provided best fuel efficiency result for the DP method compared to the heuristic strategy and rule based strategy. Rig tests later performed showed differences compared to simulation. Measured fuel consumption reduction and robustness towards driver variance was significantly better for the heuristic strategy. The DP method had larger variance in the fuel consumption between each test and driver but showed overall improvements compared to the rule based strategy without look-ahead information.

Paper III

Three different optimization methods are compared for a series plugin hybrid electric vehicle, all of them utilizing look-ahead information. The different methods are varied with different operating modes. The first method assumes that running the engine in one operating point (the highest system efficiency) is always the optimum. Thus the optimization consists of finding the segments in the drivecycle for where the engine should provide electrical power. Method 2 can control the charging

power freely within one segment and speed is controlled efficiently to the optimum operating line with a rule based speed controller. Method 3 does not limit the engine towards the optimum efficiency line when requesting a new engine power request, instead running at other speeds outside the optimum efficiency line or optimum system efficiency point. The control signals are the engine torque and generator power. Method 3 is more computationally intensive than Method 1 and Method 2. In order to reduce the computational effort for all methods a reachability analysis was carried out, simulating the model forward and backwards in time with controller input set to maximum or minimum setpoint levels. For the 2-state DP algorithm this reduced from 11.4 million iterations to 33573 iterations. The simulation result showed that lowest fuel consumption was obtained by Method 3 (2-dimensional). The load following method was less fuel efficient than the constant load approach. Battery cycling was shown to be best for the load following approach but the overall RMS current was lower for load and speed varying method. The most interesting finding was that due to engine dynamics, it is not always beneficial to run the engine at the best efficiency point.

5
Future Work

The work until now has consisted of high level control of energy distribution under a drivecycle. Near term studies will focus more on short horizon decisions. That is: how vehicle speed, torque split and gears can be controlled more efficiently together. Moreover it will be tested how infrastructure can be used to improve emission and light-off for catalysts.

5.1 Optimal speed and gear selection with look-ahead information

The problem of controlling gear and speed has been carried out since 1977 [47]. Methods have since then been developed to solve the problem with different gears or gear ratios for combustion engines [54], [55], [38] and optimum vehicle speed for electrified drivetrains [36]. Tests performed on trucks [27] have shown a significant fuel saving potential. The problem is illustrated in Figure 5.1 where a vehicle is travelling over a hill and incorporates minimizing fuel consumption by controlling gears and torques such that the vehicle speed remains within operational limits when look-ahead information is known.

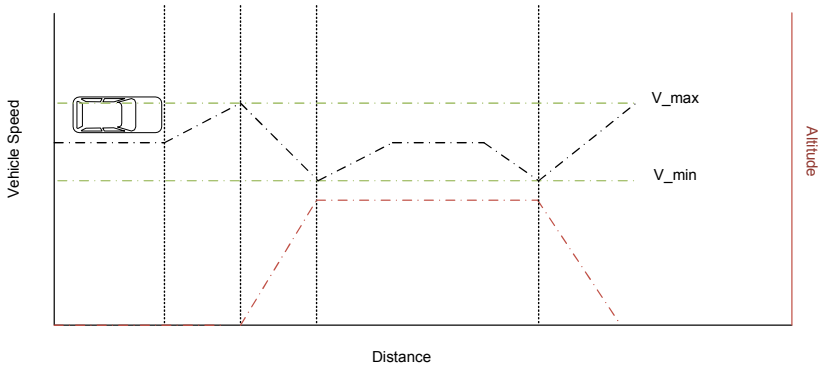

Figure 5.1: Vehicle optimum speed driving up and down a hill

As highlighted in [7] there are still factors that are preventing a real world implementation for more energy efficient control of vehicles. First: Many methods are

too computationally intensive for a vehicle ECU or unable to provide good results with map data differences to real world or other disturbances related to vehicle, driver, weather and traffic. We have seen that a power based dynamic programming method was sensitive to disturbances in Paper II. Little research has been focusing on illustrating how sensitive different methods are regarding the previous mentioned aspects. In the future work real world implementations will be tested in a vehicle using ideas from [27] and develop this further to take engine response into consideration and combine the knowledge and opportunity to involve electric drivetrain components [36]. Simulations will be done to study the optimal solution and rig tests will be carried out to measure the influence of disturbance factors.

5.2 Predictive traffic light information influence on catalyst performance in real driving

Connected infrastructure provides new possibilities regarding optimal speed control for self driving cars, green light optimal speed is one application that uses traffic light information to adapt the speed and traffic flow of all the vehicles to avoid standstill and maximize throughput in an intersection, typically self-driving cars or vehicles driving in ACC mode. An investigation will be carried out how catalyst performance is affected during takeoff if engine start can be triggered by a traffic light instead of driver triggered engine start. An investigation of engine response, emissions and driver behavior will be conducted of a selected group of users where this function is tested with and without traffic light information during start events at crossroads. The assessment will be carried out in real traffic and reaction times, initial accelerator-pedal position, emission performance, robustness and latencies will be measured.

Bibliography

[1] ACEA. Share of Diesel Cars in Europe 1990 - 2016, 2017.

[2] ACEA. The Automobile Industry Pocket Guide. Technical report, European Automobile Manufacturers Association, Brussels, 2017.

[3] ACEA. Vehicles in use Europe 2017. Technical report, European Automobile Manufacturers Association, Brussels, 2017.

[4] Assad Alam, Jonas Mårtensson, and Karl H. Johansson. Experimental evaluation of decentralized cooperative cruise control for heavy-duty vehicle platooning. *Control Engineering Practice*, 2015.

[5] Rickard Arvidsson, Viktor Larsson, Markus Ekström, and Anette Westerlund. An Evaluation of Discharge Strategies for Plug- In Hybrid Electric Vehicles. *25th Aachen Colloquium Automobile and Engine Technology*, 2016.

[6] Rickard Arvidsson and Tomas McKelvey. Battery parameter estimation from recorded fleet data. In *SAE Petrols and Fuels*. Signals and Systems, SAE, 2016.

[7] Zachary D. Asher, V Wifvat, Anthony Navarro, S Samuelsen, and Thomas H. Bradley. The Importance of HEV Fuel Economy and Two Research Gaps Preventing Real World Implementation of Optimal Energy Management. *SAE technical paper*, 2016.

[8] David Barber. *Bayesian Reasoning and Machine Learning*. Cambridge University Press, 2012.

[9] Richard E. Bellman. The Theory of Dynamic Programming, 1954.

[10] Richard E. Bellman. Dynamic Programming and Lagrange Multipliers. In *Proceedings of the National Academy of Sciences*, 1956.

[11] Richard E. Bellman and Stuart E Dreyfus. Applied Dynamic Programming. Technical report, Rand Corporation, Princeton, 1962.

[12] C R Birkl and D a Howey. Model identification and parameter estimation for LiFePO 4 batteries. *IET Hybrid and Electric Vehicles Conference 2013, HEVC 2013*, pages 1–6, 2013.

[13] Christopher M Bishop. *Pattern Recognition and Machine Learning*, volume 16. Springer, Cambridge, 2007.

[14] Bloomberg New Energy Finance. Electric vehicle outlook 2017, 2017.

[15] N Bowerman. Why should the government be concerned with ADAS? In *iMechE: Vehicle Control for the Future*, London, 1999. Institution of Mechanical Engineers.

[16] Arthur Earl Bryson and Yu-Chi Ho. *Applied optimal control: optimization, estimation and control*. Taylor & Francis, 1975.

[17] B Dawoud, E Amer, and D Gross. Experimental investigation of an adsorptive thermal energy storage. *International Journal of Energy Research*, 2007.

[18] Paul Dekraker, Mark Stuhldreher, and Youngki Kim. Characterizing Factors Influencing SI Engine Transient Fuel Consumption for Vehicle Simulation in ALPHA. *SAE International Journal of Engines*, 10(2):2017–01–0533, 2017.

[19] E W Dijkstra. A Note on Two Problems in Connexion with Graphs. *Numerische Mathematik 1*, (1):269–271, 1959.

[20] Gerben Doornbos. *Lean homogeneous combustion and NO x emission control for SI-engines*. Doctoral thesis, Chalmers University of Technology, Gothenburg, 2017.

[21] European Environment Agency. *Air quality in Europe — 2016 report*. Number 13. European Environment Agency, Luxembourg, 2016.

[22] European Environment Agency. *Air quality in Europe — 2017 report*. European Environment Agency, Luxembourg:, 2017.

[23] European Parliament. Average Specific CO2 and specific emission targets, 2016.

[24] European Union. *Energy, transport and environment indicators*. 2016.

[25] Exxon Mobil. 2017 Outlook for Energy. Technical report, Exxon Mobil Corporation, Irving, 2017.

[26] James A Griffiths, Peter R; De Haseth. *Fourier transform infrared spectrometry*. John Wiley & Sons, New Jersey, 2 edition, 2007.

[27] Erik Hellström. *Look-ahead Control of Heavy Vehicles Look-ahead Control of Heavy Vehicles*. Doctoral thesis, Linköping University, 2010.

[28] John B Heywood. Internal Combustion Engine Fundamentals. In *Internal Combustion Engine Fundamentals*. McGraw Hill, 1988.

[29] Yuto Imanishi, Naoyuki Tashiro, Yoichi Iihoshi, and Takashi Okada. Development of Predictive Powertrain State Switching Control for Eco-Saving ACC. In *WCX™ 17: SAE World Congress Experience*. SAE International, 2017.

[30] International Organization for Standardization. ISO 16183:2002. Technical report, International Organization for Standardization, Geneva, 2002.

[31] Ho Gi Jung, Yun Hee Lee, Pal Joo Yoon, and Jaihie Kim. Forward Sensing System for LKS+ACC. In *SAE World Congress & Exhibition*. SAE International, 2008.

[32] Shengbo Eben Li, Huei Peng, Keqiang Li, and Jianqiang Wang. Minimum fuel control strategy in automated car-following scenarios. *IEEE Transactions on Vehicular Technology*, 61(3):998–1007, 2012.

[33] Kuo Yun Liang, Jonas Mårtensson, and Karl H. Johansson. Heavy-Duty Vehicle Platoon Formation for Fuel Efficiency. *IEEE Transactions on Intelligent Transportation Systems*, 2016.

[34] Magnus Lindgren. A transient fuel consumption model for non-road mobile machinery. *Biosystems Engineering*, 91(2):139–147, 2005.

[35] Yintong Liu, Liguang Li, Haifeng Lu, Jun Deng, and Zongjie Hu. In-Cycle Knocking Detection and Feedback Control Based on In-Cylinder Pressure and Ion Current Signal in a GDI Engine. *SAE Technical Paper*, pages 2016–01–0816, 2016.

[36] Dongbin Lu, Minggao Ouyang, Jing Gu, and Jianqiu Li. *Optimal Velocity Control for a Battery Electric Vehicle Driven by Permanent Magnet Synchronous Motors*, volume 2014. Hindawi Publishing Corporation, Beijing, 2014.

[37] Jianbo Lu, Sanghyun Hong, Jonathan Sullivan, Guopeng Hu, Edward Dai, Dennis Reed, and Ryan Baker. Predictive Transmission Shift Schedule for Improving Fuel Economy and Drivability Using Electronic Horizon. *SAE Int. J. Engines*, 2017.

[38] Ilya Kolmanovsky Luigi Del Re, Frank Allgöwer, Luigi Glielmo, Carlos Guardiola. *Automotive Model Predictive Control: Models, Methods and Applications*. Springer, 2010.

[39] Peter Mock. Real-driving emissions test procedure for exhaust gas pollutant emissions of cars and light commercial vehicles in Europe. *International Council on Clean Transportation*, 2017.

[40] A.K. Oppenheim. The Knock Syndrome — Its Cures and Its Victims. In *Fuels and Lubricants Meeting & Exposition*, Baltimore, 1984. SAE.

[41] Engin Ozatay, Umit Ozguner, John Michelini, and Dimitar Filev. Analytical solution to the minimum energy consumption based velocity profile optimization problem with variable road grade. *IFAC Proceedings Volumes (IFAC-PapersOnline)*, 19(2005):7541–7546, 2014.

[42] P. Plötz, S. A. Funke, P. Jochem, and M. Wietschel. CO2 Mitigation Potential of Plug-in Hybrid Electric Vehicles larger than expected. *Springer Nature*, 7(1):16493, 2017.

[43] Vitaly Y. Prikhodko, James E. Parks, Josh A. Pihl, and Todd J. Toops. Ammonia Generation and Utilization in a Passive SCR (TWC+SCR) System on Lean Gasoline Engine. *SAE International Journal of Engines*, 9(2):2016–01–0934, 2016.

[44] Derek Rotz, Alexander Bracht, Ole Henry Dorum, Kevin Moran, and James Lynch. Quality Assurance and Robustness for Predictive Cruise Control Using Digital Map Data. In *SAE 2010 World Congress & Exhibition*. SAE International, 2010.

[45] Roman Schmied, Harald Waschl, and Luigi Re. A Simplified Fuel Efficient Predictive Cruise Control Approach. In *SAE 2015 World Congress & Exhibition*. SAE International, 2017.

[46] M Schori, T J Boehme, B Frank, and M Schultalbers. Calibration of parallel hybrid vehicles based on hybrid optimal control theory. *9th IFAC Symposium on Nonlinear Control Systems, NOLCOS 2013*, 9(PART 1):475–480, 2013.

[47] A. B. Schwarzkopf and R. B. Leipnik. Control of highway vehicles for minimum fuel consumption over varying terrain. *Transportation Research*, 11(4):279–286, 1977.

[48] Paul H Schweitzer and Thomas W Collins. Electronic Spark Timing Control for Motor Vehicles. Technical Report 780655, Optimizer Control Corp., Warrendale, 1978.

[49] Antonio Sciarretta, Michael Back, and Lino Guzzella. Optimal control of parallel hybrid electric vehicles. *Control Systems Technology, IEEE Transactions on*, 12(3):352–363, 2004.

[50] Seyed Mohammad Reza and Hashemi Mogaddam. The Use of Fuzzy Controller for Optimizing the Brake Performance. In *Proceedings of the 20th Annual Brake Colloquium and Exhibition*, number 724, Phoenix, 2002. SAE International.

[51] Xun Shen, Yahui Zhang, Tielong Shen, and Chanyut Khajorntraidet. Spark advance self-optimization with knock probability threshold for lean-burn operation mode of SI engine. *Energy*, 122:1–10, 2017.

[52] Brian C. Smith. *Fundamentals of Fourier transform infrared spectroscopy, 2d ed.* Portland, 2 edition, 2011.

[53] Stockholm Stad. Luften i Stockholm, Årsrapport 2011. Technical report, Miljöförvaltningen i Stockholm, Stockholm, 2011.

[54] Ap Stoicescu. On fuel-optimal velocity control of a motor vehicle. *International Journal of Vehicle Design*, 16(2):229–56, 1995.

[55] A.P. Stoicescu. Time-optimal velocity control of a motor-vehicle with CVT. *International Journal of Vehicle Design*, 30(4), 2002.

[56] Xidong Tang, Xiaofeng Mao, Jian Lin, and Brian Koch. Li-ion battery parameter estimation for state of charge. *American Control Conference (ACC), 2011*, pages 941 – 946, 2011.

[57] Kotub Uddin, Surak Perera, Widanalage D Widanage, and James Marco. Characterising Li-ion battery degradation through the identification of perturbations in electrochemical battery models. In *EVS28 International Electric Vehicle Symposium and Exhibition*, volume 28, pages 1–9, Coventry, 2015. The University of Warwick.

[58] Martin Weiss, Pierre Bonnel, Rudolf Hummel, Urbano Manfredi, Rinaldo Colombo, Gaston Lanappe, Philippe Lelijour, and Mirco Sculati. Analyzing on-road emissions of light-duty vehicles with Portable Emission Measurement Systems (PEMS). Technical report, European Commission, Luxembourg, 2011.

[59] Byeong Wook, Dong Hoon, Young-il Chang, and Sang-Hwan Kim. Development of Smart Shift & Drive Control System based on the Personal Driving Style Adaptation . In *SAE 2016 World Congress and Exhibition*. SAE International, 2016.